UNIVERSITYOF BIRMINGHAM

University of Birmingham
Research at Birmingham

Experimental investigation of the aerodynamics of a freight train passing through a tunnel using a moving model

Iliadis, Panagiotis; Soper, David; Baker, Christopher; Hemida, Hassan

[Link to publication on Research at Birmingham portal](#)

Corresponding Author:

Panagiotis Iliadis, Department of Civil Engineering, School of Engineering, University of Birmingham, Edgbaston, Birmingham, B15 2TT, UK

E-mail: pxi563@bham.ac.uk

Experimental investigation of the aerodynamics of a freight train passing through a tunnel using a moving model

P. Iliadis, D. Soper, C. Baker, H. Hemida*

*Department of Civil Engineering, School of Engineering, University of Birmingham, Edgbaston, Birmingham, B15 2TT, UK

Abstract

The objective of this study was to investigate the aerodynamic effects of a freight train passing through a tunnel. The nose entry generates a complex pattern of reflective pressure waves (piston-effect) which can lead to intense aerodynamic forces. Previous research on the topic has focused on passenger trains because of higher speeds. The experiments of this study use a 1/25th scaled moving model at the TRAIN Rig at a speed of 33.5m/s with a blockage ratio of 0.202. The monitored pressure along the tunnel wall can increase up to almost 1000Pa because of the initial compression wave, while it drops when an expansion wave or the tail passes by. The maximum pressure is observed at the train nose due to air stagnation (1500Pa) where the flow is steady, while the roof and sides experience negative pressures due to unsteady flow separation. The effect of loading configuration is significant as partially loaded trains can create a second pressure peak on the tunnel walls (after the initial compression wave) and affects the flow at the tunnel entrance wall. Under the current testing conditions, the results indicated compliance with the requirements of the TSI and a constant pressure gradient of the initial compression wave which is in contrast with passenger trains' two-part gradient. Further work on the topic could provide visual information about the exiting jet towards the portal and the separation bubble around the train.

Keywords

Freight train, Compression wave, Aerodynamics, Moving model, Piston-effect

1. Introduction

Recently researchers have shown interest in freight train due to plans for increasing the capacity of railway systems, where increasing speeds is the most efficient response.[1, 2] Up to now, the majority of train aerodynamics research has tended to focus on passenger trains rather than on freight trains. The focus on higher speed passenger trains [3-5] is justified by the fact that in very broad terms the aerodynamic forces in open air conditions present a proportional relation to the square of velocity.[6] More specifically, when a train travels at 250-300 km/h, 75-80% of the total resistance is caused by drag.[7] Consequently, amplitudes of

pressure change proportionally to the square of speed.[8] However, when a train enters a tunnel, additional amounts of drag are present [9] as a repeated pattern of reflective pressure waves is formed. The drag inside the tunnel is divided into skin friction and pressure drag. Skin friction drag increases with higher blockage ratio, train length and surface roughness [10] while the pressure waves inside the tunnel generate drag as they contain energy. The additional drag inside the tunnel is translated to a tunnel friction factor[11] which can be related to the drag coefficient in open air.[12] As a result, the additional amount of drag reduces the aerodynamic efficiency. Nonetheless, aerodynamic efficiency is not the only consequence of the pressure waves formation. The intense aerodynamic forces produced from the pressure waves can cause structural and stability problems on the train and track.

The effects mentioned above, make it essential to investigate in detail the nature of the generated pressure waves and their interaction with the 'blunt' nose and the rough discontinuous sides of a freight train. The pressure waves take the form of a complex pattern of compressive and expansive waves. The nose of the train pushes the air ahead of it, and generates a compression wave.[13] The wave travels with the speed of sound, and then reflects back as an expansive pressure wave similarly to an open-end piston effect.[14] Then it follows a repeated pattern of reflective waves which change sign during reflection. Therefore, the initial compression during nose entry produces the highest magnitude of pressure increase and the most intense pressure gradient. As a result, several researchers have focused on the development of the initial compression wave using 1-D analytical theory.[15] Such studies highlight the effects of the train nose, encouraging the investigation of a freight train, since the nose coefficient for freight trains is significantly higher compared to passenger trains. However, if the initial compression is not the only focus of the investigation, alternative methods are used such as experiments and Computational Fluid Dynamics (CFD).[9, 16] These methods can predict the complete pressure waves pattern which becomes more complex when the tail enters the tunnel. During the tail's entry, an expansive pressure wave is generated, traveling until the exit of the tunnel and then reflects as a compression wave. During the reflection, a small part of the pressure wave is radiated to the environment as micro-pressure wave. The micro-pressure waves are pulses of pressure emitted to environment and at high speeds they can generate noise up to 140-150Db becoming environmentally harmful.[17] They are caused by nonlinear steepening and their amplitude depends on the gradient of the initial compression wave.[17, 18] The initial pressure gradient mainly depends on the shape of the tunnel entrance portal, the blockage ratio, the train speed and the train nose. Therefore, the steepness of the initial wave pressure gradient must be reduced (i.e. using a slanted entrance).[19] There is a strong variation of the magnitude of the micro-pressure waves with speed. More specific, noise emissions are a particular problem with high speed trains in excess of 250 km/h.[20] The extent to which the micro-pressure waves are emitted to the environment directly influence the attenuation of the pressure waves inside the tunnel (because some energy is lost to the environment), and therefore they should not be ignored. Having discussed the generation and reflection of the pressure waves in detail, it must be mentioned that the generation of pressure waves is not the only effect of the nose entry. Some of the air particles are pushed ahead but they run backwards around the train and travel towards the tunnel entrance.[21] This phenomenon stops when the train tail is completely inside the tunnel.[22]

The nose pushes the air molecules ahead of it and generates a pressure wave. Then this wave-front of high pressure travels at the speed of sound until the end of the tunnel where reflection occurs. The high pressure of the planar wave occurs due to the fact that the air molecules are closer to each other (compression wave). The pressure waves reflect similarly to the reflection of an open-end pipe due to the piston movement. Impedance mismatch is the

reason behind wave reflection. Acoustic impedance (or flow impedance) is defined as the ratio of sound pressure to volumetric flow rate.[23] More specifically, for a pipe:

$$Z = \frac{p}{Ac} \tag{1}$$

Eq. (1) shows the direct dependence of impedance to the cross-section area. When the wave reaches the exit of the tunnel, the sudden increase in cross section area reduces the value of acoustic impedance. The impedance mismatch at the boundary of the tunnel exit causes the reflection of the pressure wave. Impedance drops to a lower value and therefore changes the sign of the pressure wave (a compressive wave turns into an expansive wave and vice versa). The maximum pressure changes occurring in the tunnel have been specified in TSI[24], expressed in terms of the initial compression wave which is divided into two parts; the steep gradient increase Δ_{pN} caused when the nose enters the tunnel and the second pressure increase Δ_{Fr} when due to friction effects when the main part of the train enters the tunnel.[11]

Table 1: TSI Requirements

Train type	Reference case		Criteria for the reference case	
	V [m/s]	A [m^2]	Δ_{pN} [Pa]	$\Delta_{pN} + \Delta_{Fr}$ [Pa]
$V_{tr,max} \leq 69.4$ m/s	55.5	53.6	≤1750	≤3000
$V_{tr,max} \geq 69.4$ m/s	69.4	63	≤1600	≤3000

This study investigates the pressure gradient and amplitude caused by the blunt nose of the freight train, the effect of train length and loading configuration as well as the compliance of a freight train with current regulations. The tests are conducted in line with the testing methodologies as specified in CEN.[11]To that end, the data have been obtained using model-scale experiments which aim to provide detailed pressure and velocity data inside and outside of the tunnel, as well as on the surface of the moving train. The following cases are tested:

a. A Class 66 locomotive connected to 4 fully loaded container wagons where pressure is recorded at the tunnels walls, train surface, at the entrance wall. The data aims to illustrate the maximum pressure changes occurring at the tunnel walls, and the exact pressure forces experienced by the train. Additional measurements at the entrance of the tunnel show important information for tunnel and train design, as well as investigating the compliance of freight trains operation with current regulations for tunnels.

b. The effect of train length on the tunnel pressure histories is investigated using an 8-wagon train. The length is believed to influence a number of flow effects such as the interaction between the pressure waves with each other, the emission of micro-pressure waves (and thus the attenuation of the sound waves) and the flow at the tunnel portal.

c. The extreme case of 33% loading is tested. A previous study by Soper, Baker and Sterling has shown that the flow around the train in open air conditions (slipstream) is significantly influenced by different loading configurations.[1]

The long-term aim is to provide aerodynamic data which can be used for future freight train and tunnel design. More aerodynamically efficient freight trains could contribute to reducing CO_2 emissions by replacing less efficient (hence environmentally harmful) modes of

transport such as truck freight. The lack of aerodynamic data for freight trains in tunnels make this study necessary.

2. Methods

Physical simulations are performed using a moving model at the TRAIN Rig facility where the scale of the model is 1/25. The TRAIN Rig is 150m long and the model is fired by a mechanical propulsion system, composed by tensioned elastic ropes. The measurements take place at a steady speed section until the train is brought to rest by a piston deformable tube braking system. The term 'train' in this study refers to a Class 66 locomotive which is connected to FEA type B wagons carrying containers. Simplifications were made both on the locomotive and wagons, and more details about them can be found in the study of Soper, Baker and Sterling[1]. The shape of the train nose and front cross-sectional area have been retained, as these are believed to be the main factors influencing the development of the pressure waves in the tunnel. The bogie region is highly simplified and it is accepted that the flow at this region will differ from the real full scale train. Similarly, the underbody region of the FEA wagons is simplified at the same level. The current scaled model has been used in the study of Soper [25] for slipstream measurements where the shape of the train at the sides, roof and underbody play a significant role, and satisfactory agreement with full scale data was obtained. The scaled locomotive is 0.85m long, 0.106m wide and 0.156m high, while the wagons have a length of 0.8m. For the partially loaded case, a number of containers were removed. The remaining containers were placed in the middle of the each flatbed, representing 33% of the fully loaded case (by volume).

2.1 Measurement equipment and positions

Tunnel surface measurements: The pressure taps are perpendicular to the flow direction, directly connected to the piezoresistive amplified differential low pressure sensors. The sensors are capable to record for a range of ±2500Pa and their hysteresis error is ±0.05. The voltage (V) output is zeroed with respect to the first 1000 samples and converted to Pascal (Pa) using equations calculated from a series of Betz anemometer calibrations. Data is recorded with a frequency of 1000Hz using a 16-channel data logger. It consists of four-measurement locations across the tunnel length (22.98m long) at 2, 4, 8 and 16 metres away from the entrance. Three measurements points along the radius of the tunnel are monitored to confirm the continuity of the pressure waves in this direction. Previous studies have shown that the pressure waves are essentially planar.[26] As the data presents consistency between subsequent runs, three runs are adequate for sampling.

Locomotive surface measurements: The pressure history on the surface of the moving train provide useful information about the separation around the train and its interaction with the reflective pressure waves. Holes are drilled on the train surface where the metal adapters are fitted, acting as pressure tapping. The sensors are connected to the metal adapters through a plastic tube. The tube has an inner diameter of 0.16mm inner and is 25cm long and has temperature and pressure handling abilities. A correction has been applied using the inverse tubing system transfer function to account for distortion effects. The correction method uses a speaker system to sweep through different frequency ranges to highlight any issues. The on-board system is shown in Figure 1. The in-house data logger records data with a frequency of 4000Hz while the results are ensemble averaged over a minimum sample of 15 runs due to the turbulent nature of the flow. 9 pressure taps are placed on the nose, and 20 pressure taps at the side and roof of the locomotive. Both sides of the train are tested, for capturing 3-Dimensional effects such as vortices. Moreover, a light detector is fitted on the locomotive,

connected to the 16th channel of the logger. It detects the light sources at the entrance and exit boundaries of the tunnel for recording the train location.

Entrance wall measurements: The exit jet towards the tunnel portal can be captured, showing the influence of the approaching train and post-entry effects. 11 pressure taps are placed in the entrance wall, with increasing distance from the train (see Figure 1). The sensor port is fitted directly into the drilled hole of the wall and then to the data logger which record with a frequency of 1000Hz.

2.2 Similarity criteria

The use of a reduced scaled model arises from the complexity and cost of full-scale experiments in tunnels. Reynolds number and Mach number are the similarity parameters for viscosity and compressibility respectively. Reynolds number is the ratio of inertial to viscous forces. Using a Reynolds number which is close to the full-scale tests can capture the effects of viscous forces correctly. The open track railway aerodynamics requirements state that a minimum of 250,000 Re should be used to represent full scale tests. [27] According to CEN train experiments can be conducted with a minimum of 1/25 scale, for minimizing Reynolds number effects. [11] Previous studies have confirmed the validity of this minimum size for the flow field around passenger trains[28] and for trains in tunnels through comparison to full-scale data. Johnson and Dalley have conducted 1/25th scaled experiments for a passenger train passing through a tunnel at the TRAIN RIG, and the comparison of pressures inside the tunnel with full scale results showed excellent agreement.[29] Similar experiments to the current study have been successfully performed recently by Zhang et al.[30] using a scaled moving model. The pressure amplitudes do not change in full scale, but the pressure traces in the scaled tunnel occur 25 times faster than in full scale. The Re number of this test is 384,000 and its calculation is based on the height of the scaled model. When conducting scaled tests on trains in tunnels with Re>360,000, the similarity criterion is satisfied.[13, 30, 31, 32, 33] Mach number is a similarity parameter for the compressibility of the air. According to CEN, the full-scale Mach number must be respected for speeds up to 0.3, although the characteristic length changes.[11]

Apart from the prediction of the pressure waves, the Reynolds number effects on the separated flow around the train is of significant interest. When investigating the flow around the train in open air (slipstream) using the current scaled model in the TRAIN Rig facility, the boundary layer growth and velocity/pressure magnitudes are comparable in full and model scale.[25] However, the same study suggests that different Reynolds number influences at which scales dissipation occurs, and the finer small turbulent scales are different. Therefore, the results can only be used to offer an insight into key flow characteristics.

Table 2: Parameters - Full scale unless stated otherwise

Locomotive	Class 66
Container wagons	FEA Type-B
Number of wagons	4 & 8
Total scaled-train length	99.75 & 182m (respectively)
Model scale	$\dfrac{1}{25}$

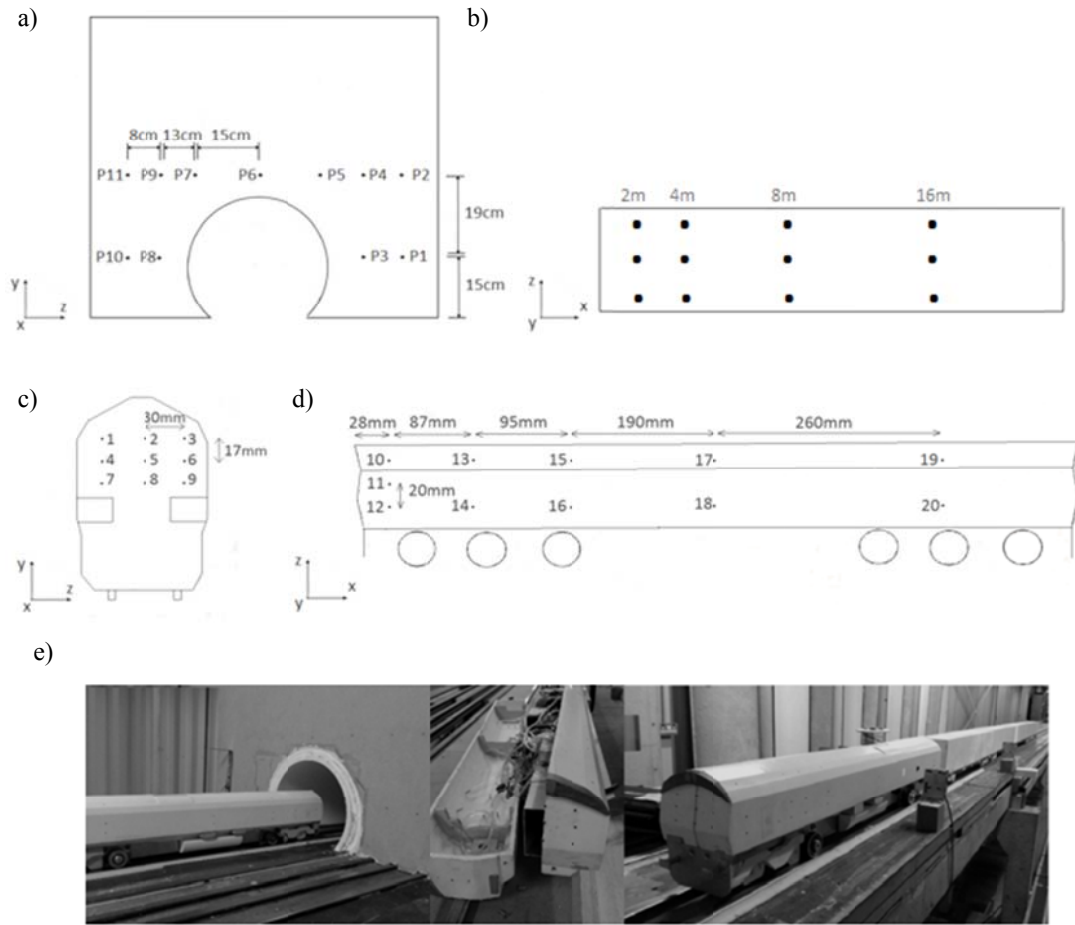|	
Train cross sectional area	$9.08m^2$
Tunnel length	574.5m
Tunnel cross sectional area	$45m^2$
Train speed	33.5m/s
Re (Scaled model)	384,000
Characteristic length (Scaled model)	0.156m (locomotive height)
Blockage ratio	0.202

Figure 1: Measurement points a) Entrance wall b) Tunnel walls c) Nose of the locomotive d) Roof and side of the locomotive e) Model scale train and tunnel

3. Results

The time-pressure histories are presented in terms of the train location in the tunnel. The nose enters the tunnel at time 0s with a speed of 33.5m/s followed by a speed reduction due to drag and friction. The speed is measured at the boundaries of the entrance and exit of the tunnel, thus a linear speed decrease is assumed between the two locations. All data presented in this chapter, is in scaled time-base. Multiplying the time-base of the presented results by 25 gives the full-scale values.

3.1 Nose of the train

The data on the nose of locomotive presents no significant variation between different pressure taps over this area. Thus, only two of the nose measurements points are presented in this set of data. The flow at this region is steady and inviscid, which is evident from the lack of pressure fluctuations. This is in contrast with the roof and side

data where fluctuations are large due to turbulence and separated flow. The pre-tunnel pressure at the front of the train (nose) is positive due to the flow stagnation. Pressure increases as the air is brought at rest at the wall. The air particles escape to the sides, roof and bottom of the train. During entry, the nose pushes the air inside the tunnel and generates the compression wave where the nose experiences pressures as high as 1500Pa. Decreased pressure values occur in this area only when in contact with the expansive waves. The waves become weaker after every reflection and consequently the highest pressure drop occurs with E1. In contrast to the tunnel wall data, the on-board pressure returns back to its pre-tunnel value exactly after exiting the tunnel. The pressure waves inside the tunnel do not stop until they attenuate to rest. The highest pressure amplitudes are found at the nose of the train, remaining in the positive axis. The most important parameters influencing the flow on the locomotive surface are the propagation of pressure waves inside the tunnel, their interaction with the train, and the interaction of the train with the entrance and exit portals. These phenomena can be effectively identified on Figure 2 by pointing the location of the train and the pressure waves. The diagram illustrates the location of the nose and tail in relation to the tunnel length. The first pressure waves reach faster the tunnel exit (compared to the train) as they travel with the speed of sound. The first pressure wave is compressive and changes sign (from compressive to expansive and vice versa) after every reflection. Similarly, the expansive wave due to tail entry changes its sign after every reflection.
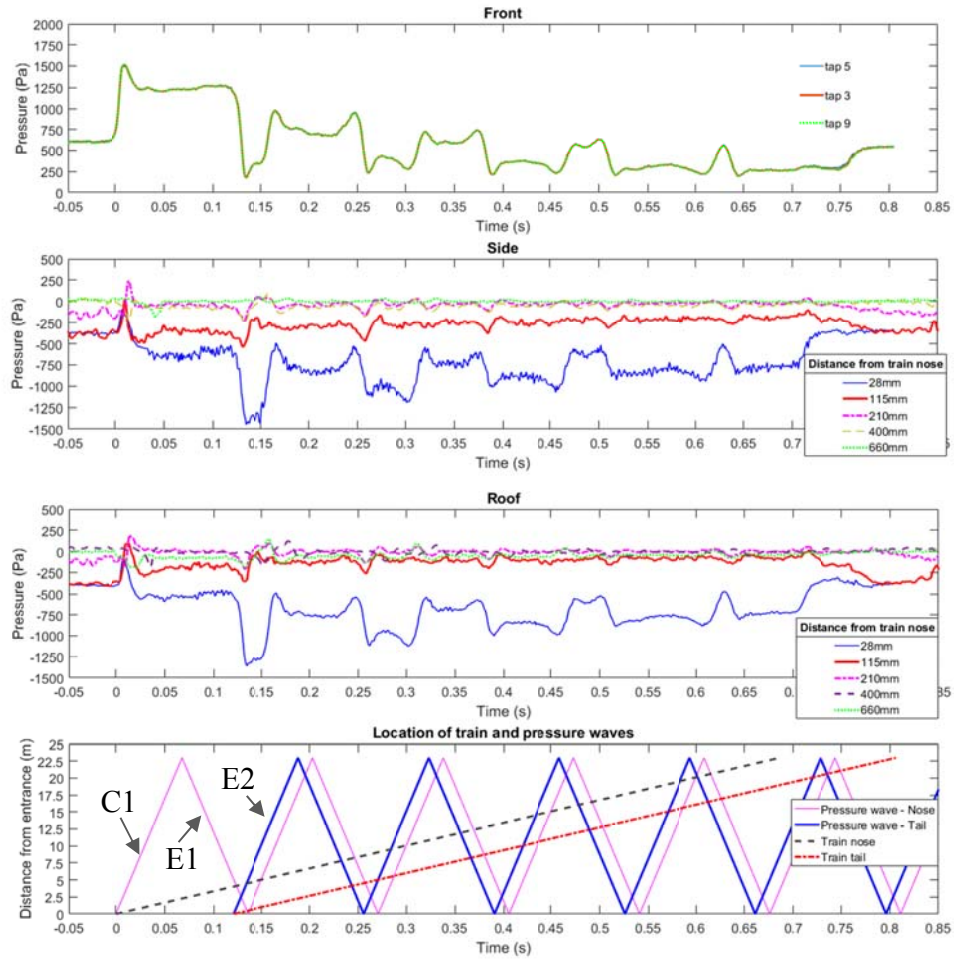
Figure 2: Pressure data on the moving surface of the locomotive connected to 4 wagons in relation to the location of the train nose, train tail and the pressure waves generated as a result of the nose and tail entry. The nose enters the tunnel at time 0s.

3.2 Roof and side of train

In contrast to the nose of the train, the pre-tunnel pressure over the roof is negative because of the reversed flow in the region. When the flow is diverted at the train nose, an adverse pressure gradient leads to flow separation. The slow air particles near the wall do not have enough inertia to overcome this opposing pressure gradient while the fast-moving particles away from the wall are more resistant. The near wall particles move backwards (reverse flow), creating a shear between the inner and outer layers. The shear rolls to form a vortex, leading to flow separation followed by a stagnant air region. Then, the particles curve back to the surface to form a reverse flow region. This region is called the separation bubble, and is represented by the plotted data at the nearest points to the nose (28 mm). As we move further away from the nose, the reattachment negative values show the reattached flow. No significant effects of the flow separation are found in the last two taps (400 & 660mm). Moving on now to consider the flow in the confined space,

the first observations arise when the nose passes the portal. The near-nose area experiences an increase in pressure followed by a sudden drop, which could be linked to a change in the nature of the separation bubble. There is experimental evidence that the bubble increases the effective blockage area and the train entry extends the length of the separation bubble by delaying the reattachment, affecting the length and height of the bubble. More specific, a 90° corner (similar to freight trains) can increase the length of the bubble up to 29%.[26] On the other hand, the rear points show a drop in pressure which could be attributed to the extension of the separation further backward. It is also believed that the jet towards the tunnel portal affects the flow at the roof and sides. As highlighted in the literature, the air near the nose is displaced during entry and travels towards the tunnel portal, experiencing friction effects both from the train and the tunnel. The amount of the displaced air depends on the blockage ratio and another set of parameters such as speed and nose shape. Auvity and Bellenoue have shown that the shear layers of this exiting jet form a vortex which stops only when the tail is inside the tunnel.[34]

Figure 3 illustrates that the meeting of the train with E2 causes a pressure drop. This drop is sharp for the near nose points but smoother for the rest of the taps. Then all taps experience rises and drops when in contact with the compression and expansion waves respectively. As mentioned earlier, these effects become weaker due to the attenuation of the pressure waves. In general, the highest pressure changes are observed for the measurement points near the nose. For the majority of the data, the pressure around the locomotive is negative, indicating separated flow. When comparing the roof to the sides of the train, the pressure histories are identical. The most noticeable differences are found at 115mm from the train nose, where the flow over the roof is affected to a greater extend when it enters the tunnel.

3.3 Stationary points along the tunnel wall

The tunnel wall data can be used for accessing the train's compliance with current regulations. As shown in Figure 3, pressure starts increasing slightly before the train's entry. When the nose enters, the air particles ahead of the train are pushed and a compressive wave forms. As the wave front passes from each measurement point, pressure increases. The amplitude of C1 is the same for all measurement points along the length of the tunnel. The maximum amplitude is approximately 1000Pa which is below the 3000Pa maximum limit for trains operating below 69.4m/s.[24] For the fully loaded cases, C1 produces the highest pressure increase in the tunnel. As a general observation, an increase is observed whenever a compression wave (high pressure) or the tail of the train passes from a measurement point. Attention must be paid when these two occur at the same time, as it can result in large pressure changes. When the tail of the train passes from the measurement point the cross-section area at the measurement position increases and velocity reduces. On the other side, a pressure drop is observed when an expansion wave or the nose of the train passes from a measurement point. As the nose approaches, the flow in front of the train pushes the air away from the measurement point and pressure drops due to suction. At 2m away from the entrance, the initial pressure increase from C1 is followed by a small drop as the wave travels towards the exit. Then a further drop occurs when then train nose passes from the measurement point, followed by a third drop when the reflected pressure wave returns back as an expansion wave. The tail

entering the tunnel generates an expansion wave which passes from the measurement point, decreasing the pressure even further. At 4m, the latter 2 drops take place at the same time as the nose and the tail expansion waves meet each other, resulting in the highest pressure drop of approximately 1000Pa. There would therefore seem to be a definite need for paying attention to combined pressure changes occurring the same time, affected by the train and tunnel length, as well as the train speed. The pressure waves meet each other at several occasions inside the tunnel. When having the same sign, constructive interference occurs where the pulses overlap and create a higher instantaneous amplitude of pressure, continuing in their direction of travel. When having opposite signs, they cancel each other and then recede. In both cases, some energy can be lost during this process. This lost energy contributes to the attenuation of the pressure waves, where their amplitudes reduce. Other factors include the thermal consumption of energy due to viscosity, which reduces the acoustic energy and the radiation of the micro-pressure waves which transmit part of the pressure waves' energy out of the tunnel.
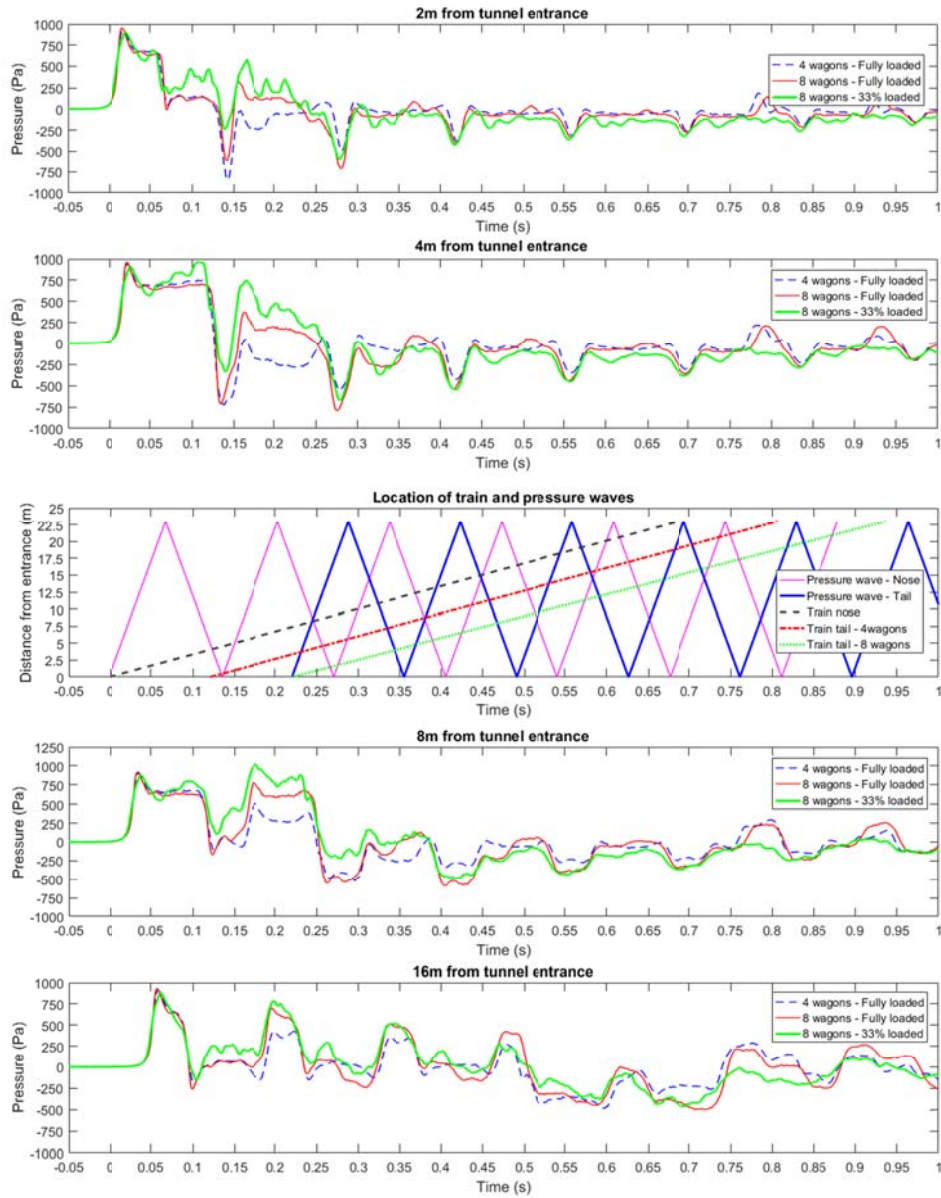
Figure 3: Pressure data along the tunnel surface (Stationary points). 4 fully loaded, 8 fully loaded and 8 partially loaded wagons are presented. The nose enters the tunnel at time 0s.

These attenuations are expected to be more significant at full-scale scale due to higher greater viscous stresses at the walls of the tunnel.[35] The reflection of the pressure waves continue even after the train tail exits the tunnel and the time period of this phenomenon depends on the train speed, blockage ratio, nose shape and train and tunnel length which influence the amplitude of C1.

3.4 Effect of train length

The development of C1 presents negligible variation with increasing the length of the train. The first differences appear when the tail of the short train (4 wagons) enters the tunnel and the expansion wave passes from the measurement point. Any minor differences can be explained by the fact that the length of the train changes the vortex ring towards the tunnel entrance, influencing the initial compression wave. The estimation of C1 using 1-D analytical models do not account for the train length.

3.5 Effect of loading

The gaps in the partially loaded wagons cause separation. This is in contrast with the fully loaded case where the flow follows the surface of the wagons (although there are small gaps between cars) and the blocked cross-sectional area is almost constant. For the 33% loaded case, intense pressure changes are monitored at stationary points in the time period between the rear part of the locomotive and train tail passage. Fluctuations are recorded, due to the complex flow pattern. These fluctuations can generate a pressure amplitude which is slightly higher than the pressure increase from C1. More specific, at 4m and 8m away from the entrance, a second peak is observed, having higher amplitude of C1. This is contradictory to all results from previous research conducted on fully loaded trains, which suggest that the highest pressure amplitude occurs at C1. This peak occurs before the nose passes from the measurement point (see Figure 3). For the same time period, the fully loaded case presents constant pressure and a smoother backward transition of the flow to the rear cars. As the main focus of analytical models is to predict the highest amplitude in the tunnel by modelling C1, this study suggests that analytical models are not used for partially loaded trains.

3.6 Entrance wall

The most significant effects are observed in the time period between the nose and tail entry, which is the focus of this entrance wall data analysis. Apart from this period of time, the only important effect observed is the pressure changes due to the arrival of the compressive and expansive waves at the entrance, increasing and decreasing the monitored pressure respectively. In this section, only the fully loaded and partially loaded cases with 8 wagons are presented (see Figure 4). The results from the 4 wagons present no significant effects apart from the delayed tail entry.
As the train approaches the tunnel, the air ahead of the nose is displaced and the pressure at the tunnel entrance wall increases. The air travels towards the tunnel interior and the entrance wall. At the wall, it is brought at rest and a stagnation area forms. The highest pressure increase is observed at P6, which is located above the centre of the track, followed by the pressure increase at P3, which are the closest points to the sides. The lowest changes are found at the upper measurement points P2 and P4, where the maximum pressure increase is approximately 20Pa. When the train is near the portal, it starts displacing the air inside the tunnel. In contrast to the open air, the air cannot move freely to the atmosphere and therefore escapes from the portal in the form of a vortex. The vortex surrounds the entrance wall and the reversed flow in this region causes a

reduction in pressure. This phenomenon becomes more intense as the nose approaches the entrance. The passing of the nose from the portal increases the pressure values at the entrance wall. The points nearer to the centre of the track P6 and P3 have a stronger pressure rise compared to the rest of the points due to the displaced air around the roof and side of the train which diverts the exiting vortex from the tunnel. For the fully loaded case, no important effects are observed between the nose and tail entry. The flow around the train at the tunnel portal is the same as the cross-section area does not change. However, for the 33% loaded case the geometry of the passing train constantly changes as some of the wagons do not have containers. Thus, the flow around the train changes which means that it does not have a constant effect on the wall. Whenever, a loaded wagon passes from the entrance boundary, pressure increases due to the displaced air around the train diverting the vortex at the measurement points. On the other hand, whenever an empty wagon passes, less air is displaced. The fluctuations between the nose and tail entry are more intense for the points on the side of the tunnel (P1, P2, P3, P4) and less significant for P5 and P6. P2 and P4 are the points which are furthest from the train surface, and therefore the effect of air displacement is less intense. Therefore, the exiting vortex is not significantly affected in this region, keeping pressure values on the negative axis.
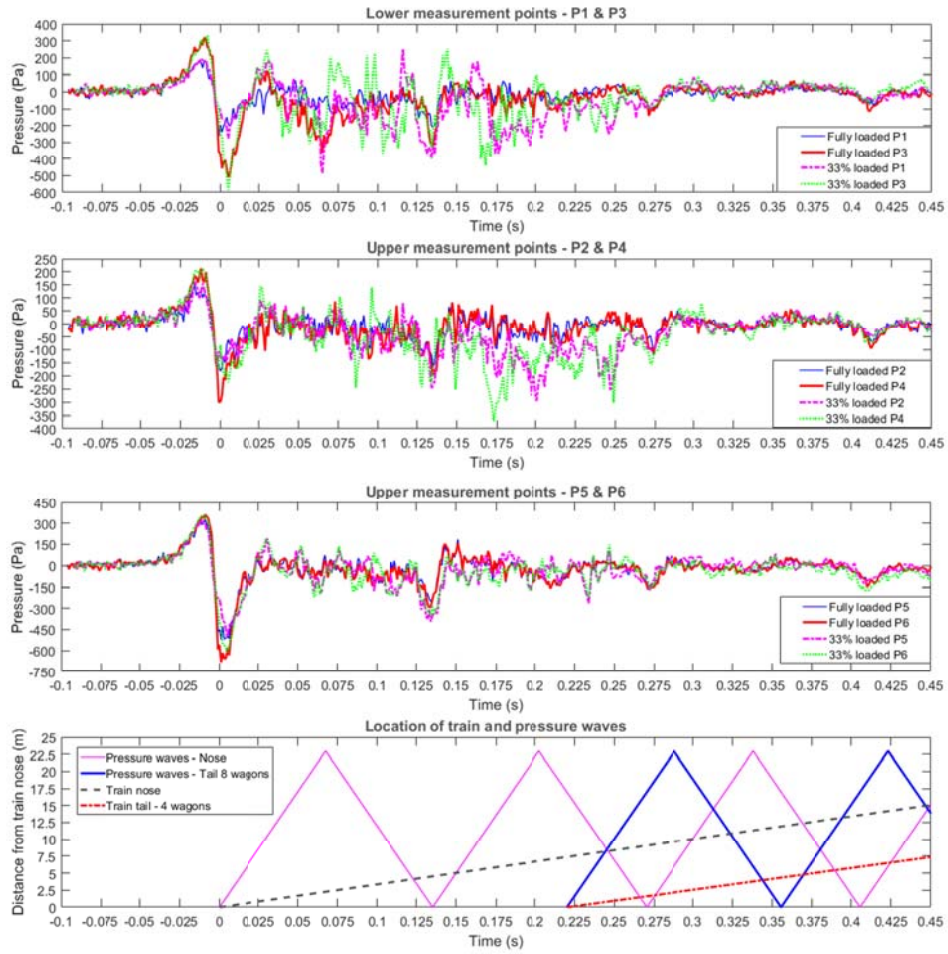
Figure 4: Pressure data at the portal wall. The locomotive is connected to 8 wagons (either fully loaded or partially loaded). The nose enters the tunnel at time 0s.

When the tail passes from the tunnel entrance and the train is wholly inside the tunnel, the effects start to attenuate and the large fluctuations stop. The graph above illustrates that when the expansion waves arrives at the tunnel entrance, the pressure at the portal reduces. This process continues until the pressure waves in the tunnel are brought to rest. In the case that two pressure waves with the same sign (compressive or expansive) arrive at the tunnel entrance with a small time difference, pressure changes due to the first pressure wave and then remains unchanged at the arrival of the second wave.

3.7 Comparison to passenger trains

The passenger train results presented in this chapter have been taken from the paper of Rety and Gregoire and adapted for a dimensionless comparison.[36] The TGV-R train has a streamlined nose which is a good representative of passenger trains. The comparison focuses on the initial compression wave because the train nose affects its shape. The occurrence of the remaining pressure waves depends on the train length, which is not

same for the two cases. For comparison purposes, both sets of data were normalized in terms of the train speed, distance from the portal and model scale. The pressure coefficient has been calculated using equation (2) based on the train speed. The time base of the scaled model has been converted to full scale. Then both sets of data were normalized using equation (3). Therefore, the results below are blockage ratio dependable.

$$C_p = \frac{P}{\frac{1}{2}\,\rho\,V^2} \qquad (2)$$

$$t^* = \frac{t}{L.c} \qquad (3)$$

As shown in Figure 5, the two trains cause an identical pressure increase inside the tunnel prior to entry. When the passenger train enters the tunnel, the front part of the nose causes the formation of initial compression wave with a certain pressure gradient. Then, the remaining of the nose length enters the tunnel and the gradual change in the geometry smoothens the gradient of the wave. Pressure rises with a certain gradient, and then reduces due to friction effects when the main body enters the tunnel. As found in the study of Choi and Kim, by changing the nose shape from blunt to streamlined, the nose length increases and the train's front cross sectional area reduces as well as the blockage ratio.[37] As a result, pressure drag is lower, in contrast with viscous drag which remained the same. The blunt nose of the Class 66 locomotive causes a pressure rise with constant gradient which is significantly steeper. The geometry changes by almost 90° which is similar to a square cube. The absence of the second gradient can be explained by the nose shape which is not elongated (to act as a smooth transition zone).
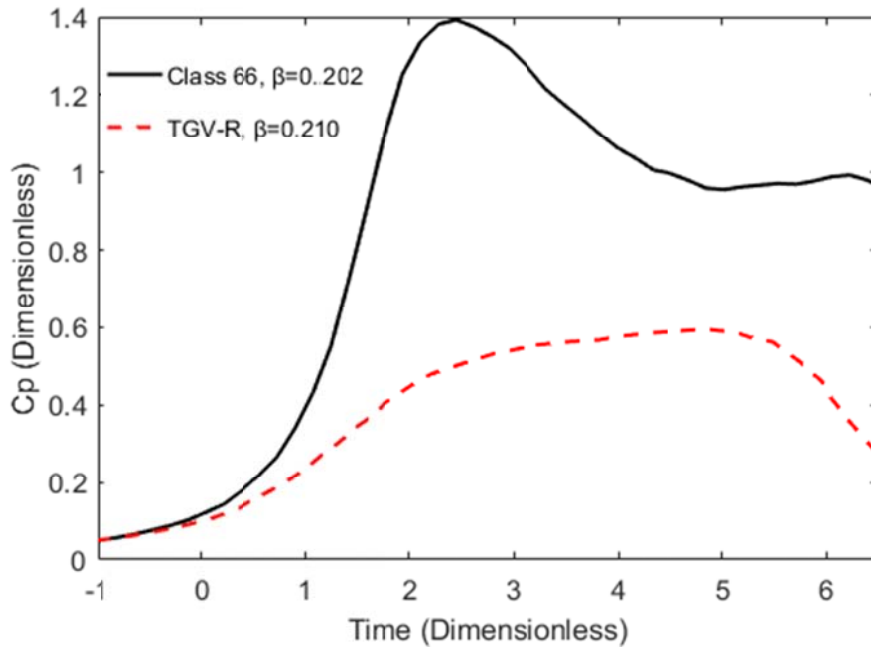

Figure 5: Initial compression wave compared to full-scale experimental data from (Rety and Gregoire, 2002) of a TGV-R into the Villejust tunnel.

The freight train causes a higher pressure rise, which is attributed to the nose shape. According to Vardy and Reinke, stagnation losses at the train nose and tail are primary sources of drag for trains in tunnels, and a relationship between the nose coefficient k_N and blockage ratio β was hypothetized.[38] The same study showed that the value of k_N for a freight train can be as high as 0.01 while for a passenger train it can be as low as 0.003. The difference in the two amplitudes is approximately 80%, which indicates strong effects of the blunt nose. The blockage ratio of TGV-R is slightly larger and the difference would be expected to be even higher if the two trains had the same ratio.

4.0 Conclusions

This study investigated for the first time the aerodynamic effects of a freight train passing through a tunnel. A $1/25^{th}$ scale moving model at the TRAIN Rig has been used, using the maximum operating speed of freight trains of 33.5m/s in line with CEN.[11] The detailed measurements presented the pressure effects along the tunnel walls, on the surface of the locomotive and the tunnel portal wall. A number of important findings are summarized as follows:

- The pressure at the tunnel wall increases whenever a compression wave or the tail passes from a measurement point and decreases when an expansion wave or the nose passes by.
- The initial pressure wave amplitude of the Class 66 locomotive at 33.5m/s with a blockage ratio β=0.202 tested under the current conditions satisfies the requirements of TSI (2014).
- The attenuation of the pressure waves is explained by the energy lost due to viscosity, the radiation of the micro-pressure waves and the interference of pressure waves. The waves continue to reflect even after the exit of the tail from the tunnel, until they run out of energy.
- It was shown that the short length of the freight train's nose causes a constant gradient initial pressure rise, contrary to passenger trains which have two gradients.
- The train nose experiences the highest pressure forces which can reach amplitudes as high as 1500Pa.
- The side and roof of the train are subject to flow separation which produces negative pressure values. The entry of the train in the tunnel has a higher influence at the near nose points of the roof and side which is evident from intense pressure fluctuations. The separation bubble extends further back towards the rear part of the locomotive after the train entry.
- In general, the interaction of the train surface with the tunnel wall has larger effects on the roof rather than the side of the train.
- For the fully loaded case, the maximum pressure amplitude occurs during the initial compression wave, in alignment with literature. On the other side, the 33% loaded train showed a second peak at the tunnel wall before the arrival of the nose to the monitor point. This new finding suggests that 1-D analytical models could not be used to predict the highest pressure in the tunnel as they only focus on the initial compression wave.

- The pressure at the tunnel portal is affected by the exiting vortex around the train and the reflected pressure waves.

The pressure experienced by the train and the pressure changes along the tunnel walls can be used as benchmark for future freight train and tunnel design. Further work could focus on using either numerical or physical simulations with visualisation (PIV or smoke) which can give further information about the exiting jet towards the tunnel portal and the separated flow around the train nose.

Funding

References

1. Soper D, Baker C and Sterling M. Experimental Investigation of the slipstream develoment around a container freight train using a moving model facility. *Journal of Wind Engineering and Industrial Aerodynamics* 2014; 135: 105-117.
2. Flynn D, Hemida H and Baker C. On the effect of crosswinds on the slipstream of a freight train and associated effects. *Journal of Wind Engineering and Industrial Aerodynamics* 2016; 156: 14-28.
3. Howe MS. Review of the theory of the compression wave generated when a high-speed train enters a tunnel. *Proc IMechE, Part F: J Rail and Rapid Transit* 1999; 213: 89-104.
4. Kwon HB, Kim TY, Lee DH, et al. Numerical simulation of unsteady compressible flows induced by a high-speed train passing through a tunnel. *Proceedings of the Institution of Mechanical Engineers, Part F: Journal of Rail and Rapid Transit* 2006; 217: 111-124.
5. Gilbert T, Baker C and Quinn A. Aerodynamic pressures around high-speed trains: the transition from unconfined to enclosed spaces. *Proceedings of the Institution of Mechanical Engineers, Part F: Journal of Rail and Rapid Transit* 2013; 227: 609-622.

6.   Baker C. A review of train aerodynamics Part 1: Fundamentals. *The Aeronautical Journal* 2014 b; 118.

7.   Peters JL. Optimizing aerodynamics to raise IC performance. *Railw Gaz Int* 1982; 138: 817-819.

8.   Li X-h, Deng J, Chen D-w, et al. Unsteady simulation for a high-speed train entering a tunnel. *Journal of Zhejiang University SCIENCE A* 2011; 12: 957-963.

9.   Novak J. Single train passing through a tunnel. In: *Proceedings of the European conference on computational fluid dynamics,* TU Delft, Netherlands, 2006, European conference on Computational Fluid Dynamics.

10.   Vardy AE. Aerodynamic drag on trains in tunnels: Part 2: Prediction and validation. *Proceedings of the Institution of Mechanical Engineers Part F Journal of Rail and Rapid Transit* 1996; 210: 39-49.

11.   CEN. EN 14067-5: 2006+A1: 2010 Railway Applications - Aerodynamics Part 5: Requirements and test procedures for aerodynamics in tunnels. CEN, 2010.

12.   Baker C. A review of train aerodynamics, Part 2 - Applications. *The Aeronautical Journal* 2014 a; 118.

13.   Bellenoue M, Moriniere V and Kageyama T. Experimental 3-D simulation of the compression wave due to train-tunnel entry. *Journal of Fluids and Structures* 2002; 16: 581-595.

14.   Howe M. *Acoustics and Aerodynamic Sound*. Cambridge University Press, 2014.

15.   Howe MS. The Compression Wave Produced by a High-Speed Train Entering a Tunnel. *Proceedings: Mathematical, Physical and Engineering Sciences* 1998; 454: 1523-1534.

16.   Ogawa T and Fujii K. Numerical investigation of three-dimensional compressible flows induced by a train moving into a tunnel. *Computers & Fluids* 1997; 26: 565-585.

17.   Shin C-H and Park W-G. Numerical study of flow characteristics of the high speed train entering into a tunnel. *Mechanics Research Communications* 2003; 30: 287-296.

18.　Howe MS, Iida M, Fukuda T, et al. Theoretical and experimental investigation of the compression wave generated by a train entering a tunnel with a flared portal. *Journal of Fluid Mechanics* 2000; 425: 111-132.

19.　Yoon TS, Lee S, Hwang H, et al. Prediction and validation on the sonic boom by a high-speed train entering a tunnel. *Journal of Sound and vibration* 2001; 247: 195-211.

20.　Maeda T. Railway technology today 9: Protecting the trackside environment. *Japan Railway & Transport Review* 1999; 22: 48-57.

21.　Auvity B, Bellenoue M and Kageyama T. Experimental study of the unsteady aerodynamic field outside a tunnel during a train entry. *Experiments in Fluids* 2001; 30.

22.　Kage K, Kawagoe S and Matsuo K. Numerical study of compression waves by high speed trains entering a tunnel. *Transanctions of JSME Series B, 58, No 547* 1992: 815-819.

23.　Mechel MP. *Formulas of Acoustics*. Springer-Verlag Berlin Heidelberg, 2008.

24.　TSI. Commission Regulation (EU) No 1302/2014 2 of 18 November 2014 concerning a technical specification for interoperability relating to the 'rolling stock - locomotives and passenger rolling stock' subsystem of the rail system in the European Union. In: Commission E, (ed.). Official Journal of the European Union, 2014.

25.　Soper D. *The aerodynamics of a container freight train*. University of Birmingham, 2014.

26.　Ricco P, Barron A and Molteni P. Nature of pressure waves induced by a high-speed train travelling through a tunnel. *Journal of Wind Engineering and Industrial Aerodynamics* 2007; 95: 781-808.

27.　CEN. Railway applications - Aerodynamics - Part 4: Requirements and test procedures for aerodynamics on open track. BSI Standards Limited, 2013.

28.　Baker C. The flow around high speed trains. *Journal of Wind Engineering and Industrial Aerodynamics* 2010; 28: 277-298.

29.   Johnson T and Dalley S. 1/25 Scale Moving Model Tests for the TRANSAERO Project. In: Schulte-Werning B., Grégoire R., Malfatti A., Matschke G. (eds) TRANSAERO — A European Initiative on Transient Aerodynamics for Railway System Optimisation. *Notes on Numerical Fluid Mechanics and Multidisciplinary Design (NNFM* 2002; 79: 123-135.

30.   Zhang L, Yang M, Liang X, et al. Oblique tunnel portal effects on train and tunnel aerodynamics based on moving model tests. *Journal of Wind Engineering and Industrial Aerodynamics* 2017; 167: 128-139.

31.   Auvity B and Kageyama T. Etude experimentale et numerique de l'onde de compression generee par l'entree d'un train dans un tunnel. *Comptes Rendus, Academie des Sciences, Serie II: Mecanique, Physique, Chimie, Astronomie* 1996; 323: 87-94.

32.   Auvity B and Bellenoue M. Effects on an opening on pressure wave propagating in a tube. *J Fluid Mech* 2005; 538: 269-289.

33.   Bellenoue M and Kageyama T. Train/tunnel geometry effects on the compression wave generated by a high-speed train. *Notes on Numerical Fluid Mechanics and Multidisciplinary Design* 2002; 79: 276-289.

34.   Auvity B and Bellenoue M. Vortex structure generated by a train-tunnel entry near the portal. In: *8th Intl Symp on Flow Visualization, Sorrento* Sorento, 1998, pp.1-4.

35.   Woods WA and Pope CW. A generalized flow prediction metthod for the unsteady flow generated by a train in a single-track tunnel. *Journal of Wind Engineering and Industrial Aerodynamics* 1981; 7: 331-360.

36.   Rety JM and Gregoire R. Numerical Investigation of Tunnel Extensions Attenuating the Pressure Gradient Generated by a Train Entering a Tunnel. *TRANSAERO — A European Initiative on Transient Aerodynamics for Railway System Optimisation Notes on Numerical Fluid Mechanics and Multidisciplinary Design (NNFM)* 2002; 79: 239-248.

37.   Choi JK and Kim KH. Effects of nose shape and tunnel cross-sectional area on aerodynamic drag of train traveling in tunnels. *Tunnelling and Underground Space Technology* 2014; 41: 62-73.

38.   Vardy AE and Reinke P. Estimation of train resistance coefficients in tunnels from measurements during routine operation. *Proceedings of the Institution of Mechanical Engineers, Part F: Journal of Rail and Rapid Transit* 1999; 213: 71-87.

Appendix

Principal symbols

A	Cross sectional area of the tunnel (m^2)
C_p	Pressure coefficient
c	Speed of sound (m/s)
L	Distance from the tunnel entrance (m)
p	Pressure (Pa)
t	Time (s)
t^*	Dimensionless time
V	Train speed (m/s)
v	Volume (m^3)
Z	Acoustic impedance (Pa·s/m^3)
ρ	Density (kg/m^3)

Subscripts

p_N	The pressure rise as the train nose enters the tunnel (Pa)
p_{Fr}	The second part of pressure rise including friction effects (Pa)
p_T	The change in pressure as the tail enters the tunnel (Pa)